Instability of Nagaoka state and quantum phase transition via kinetic frustration control

Prakash Sharma [1,2,*] Yang Peng [2,3] Donna N. Sheng [2] Hitesh J. Changlani [4,5] and Yao Wang [1]

[1]*Department of Chemistry, Emory University, Atlanta, Georgia 30322, USA*

[2]*Department of Physics and Astronomy, California State University, Northridge, California 91330, USA*

[3]*Institute of Quantum Information and Matter and Department of Physics, California Institute of Technology, Pasadena, California 91125, USA*

[4]*Department of Physics, Florida State University, Tallahassee, Florida 32306, USA*

[5]*National High Magnetic Field Laboratory, Tallahassee, Florida 32310, USA*

(Received 25 August 2025; accepted 24 March 2026; published 23 April 2026)

We investigate the Nagaoka-Thouless ferromagnetic instability in the strongly interacting t-t' Hubbard model by continuously breaking particle-hole symmetry on a tunable square-triangular lattice geometry. We use an analytic approach to show that the fully spin-polarized state becomes unstable to a metastable spin polaron when the kinetic frustration t'/t exceeds a critical, dimension-dependent value. Large-scale density matrix renormalization group simulations reveal a quantum phase transition from the Nagaoka ferromagnet to a spiral spin-density wave, which evolves continuously into the Haerter-Shastry antiferromagnet in the large-frustration limit. Remarkably, this transition remains robust at low but finite hole density, making it accessible in cold-atom and moiré Hubbard platforms under strong interactions. A variational analysis further captures the instability mechanism at finite hole density via frustration-induced magnon band deformation.

DOI: 10.1103/z4gs-c6h6

I. INTRODUCTION

Itinerant ferromagnetism (FM), proposed by Nagaoka and Thouless [1,2], arises when the motion of an itinerant electron kinetically stabilizes ferromagnetic order in an almost half-filled correlated system, which is remarkably distinct from the superexchange mechanism or the Stoner mechanism based on a mean-field instability of an interacting Fermi sea [3]. Beyond its unconventional origin, this mechanism enables direct electrical control of magnetism, as doping modulates global magnetic order by altering carrier kinetics [4,5]. It also serves as an efficient measurement for strong electronic correlations, offering a sensitive probe of the Hubbard interaction strength in moiré materials [6,7] where high-resolution single-particle spectra are inaccessible [8,9]. Furthermore, the physics of kinetic FM bridges to the double exchange mechanism observed in strongly correlated oxides [10–12], providing a unified perspective on doping-induced magnetism. While originally limited to extreme conditions in the Hubbard model, generalized forms of kinetic FM have recently been successfully realized at finite doping and experimentally accessible energy scales in moiré heterostructures [13,14] and optical lattices [15–17].

In contrast to the square lattice geometry where Nagaoka ferromagnetism (NFM) was originally predicted, recent studies have indicated the triangular lattice as a particularly compelling setting for exploring itinerant magnetism due to its inherent geometric frustration, rich phase diagram with particle-hole asymmetry [18–23], and the realizability in moiré superlattices [13,24]. In bipartite (e.g., square) lattices, a hole's kinetic energy is minimized by constructive interference along hopping pathways [Fig. 1(a)], favoring uniform spin alignment and stabilizing a conventional NFM phase [1,2]. In contrast, triangular lattices host closed loops with an odd number of bonds, inherently introducing destructive interference for certain hopping pathways [Fig. 1(b)], suppressing fully spin-polarized Nagaoka order at infinitesimal doping [25,26] and stabilizing intermediate states such as spin polarons [27–30]. Recent experiments with optical lattices and moiré heterostructures have explicitly observed a spin polaron to local Nagaoka-like ferromagnetic transition driven, respectively, by hole and particle (doublon) dopants [14–17,31], revealing fundamentally different doping dependence and transition characteristics from those observed in bipartite systems.

Despite the difference, the bipartite square lattice and geometrically frustrated triangular lattice can be gradually connected to each other by tuning one of the diagonal hopping t' in a square lattice [see Fig. 1(c)]. Since the kinetic frustration [32,33] of a hole dopant in the fully frustrated triangular limit is alleviated when the background spins adopt antiferromagnetic correlations arranged in a 120° order [25], the fundamental distinction between these two systems and their magnetic origin indicate a geometric phase transition through this lattice interpolation and potentially richer magnetic phases distinct from either ends.

To this end, we systematically investigate the instability of the Nagaoka-type ferromagnet and its evolution toward

*Contact author: sharmaprakash078@gmail.com

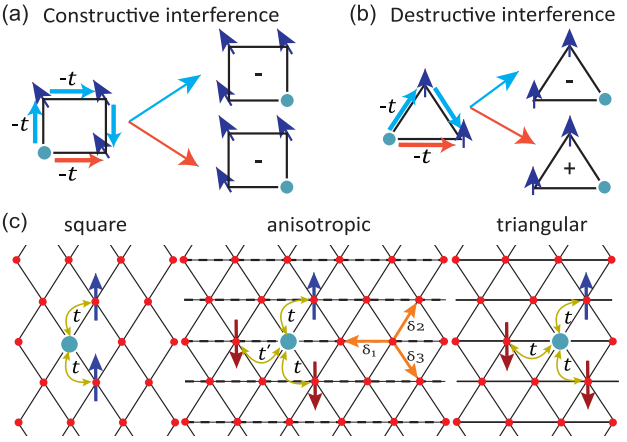

FIG. 1. Path interference of a hole in (a) a square and (b) a triangular plaquette within an FM background. On the square lattice, two hopping paths (light blue and red arrows) yield the same final configuration with identical phase and interfere constructively. On the triangular lattice with $t > 0$, two paths yield final states that differ by a fermionic sign and interfere destructively. (c) Lattice geometry interpolating between square and triangular limits. The unfrustrated square lattice has nearest-neighbor hopping t, while introducing diagonal hopping t' creates kinetic frustration. The fully frustrated triangular lattice is recovered when all bonds have equal hopping amplitude t. The nearest-neighbor vectors $\boldsymbol{\delta_1}$, $\boldsymbol{\delta_2}$, and $\boldsymbol{\delta_3}$ of triangular lattice are shown.

the low-spin antiferromagnet by continuously tuning lattice geometry from square to triangular. A similar problem has been previously explored using numerical simulations for a single-hole dopant system [34]. In this study, we combine an analytical solution with large-scale density matrix renormalization group (DMRG) to elucidate the instability mechanism and the underlying ground-state phase transition in both the single-hole-dopant and finite-hole-density cases. Our single-hole analysis also reveals that Tasaki's criteria for generalized NFM [35] are sufficient but not necessary. Most strikingly, our DMRG results beyond the idealized single-hole limit uncover that critical quantum phenomena linking NFM and the Haerter-Shastry (120° AFM) phase [25], driven by competing magnetic correlations, persist at finite-hole doping, making them directly relevant to cold-atom and moiré Hubbard experiments. We explain the physical origin of the instability of NFM at finite hole density using a simple yet insightful variational analysis, revealing that the instability emerges directly from the frustration-induced modification of dispersive magnon bands.

II. GEOMETRIC CONTROL OF KINETIC FRUSTRATION

To study the magnetism of purely kinetic origin, the $U = \infty$ Hubbard model is an ideal platform, as magnetic interactions ($J \sim t^2/U$) exactly vanish in this limit, and the model reduces to a constrained nearest-neighbor hopping,

$$\mathcal{H} = -\sum_{\langle i,j\rangle,\sigma} t_{ij} c^\dagger_{i\sigma} c_{j\sigma} (1 - n_{j-\sigma})(1 - n_{i-\sigma}) + \text{H.c.}, \quad (1)$$

where $c_{i\sigma}$ ($c^\dagger_{i\sigma}$) annihilates (creates) electron at site i with spin $\sigma = \{\uparrow, \downarrow\}$ and the projection operator $(1 - n_{i-\sigma})$ prevents from having configurations with two electrons on the same site. Consequently, electrons can only exchange positions with holes on adjacent sites.

We first consider a single-hole dopant in an otherwise half-filled two-dimensional (2D) triangular lattice with hopping strength $t_{ij} = t'$ along horizontal bonds and t otherwise [see Fig. 1(c)]. We extend the analysis to finite hole density in a later section. In the infinite-U limit, the ratio t'/t is the only tuning parameter that controls the degree of kinetic frustration, which is equivalent to a change in the lattice geometry: $t' = 0$ corresponds to a bipartite (square) lattice with particle-hole symmetry (PHS), where a single-hole-doped state exhibits NFM regardless of the sign of t. In contrast, $t'/t = 1$, with $t > 0$, corresponds to the fully frustrated triangular lattice. Such a lattice manipulation via tuning the hopping term has already been realized in cold-atom optical simulators by introducing an imbalance between two orthogonal retroreflected laser beams [21].

As parameter t', which breaks PHS continuously when tuned between 0 and t, introduces kinetic frustration for the hole, it raises the question of how the NFM ground state evolves in response to this frustration. A hole generally acquires different hopping phases depending on the sign and strength of t' (assuming $t = 1$ fixed). For example, when $t' < 0$, NFM continues to persist due to the product of the hopping phase around a triangular loop being positive [33]. This extends NFM to broader graph structures beyond bipartite geometries, as generalized by Tasaki in Ref. [35]. The more intriguing regime occurs when $t' > 0$, where an FM state competes with AFM correlations as t' increases. In this scenario, a hole may favor one or more spin flips along its path to reduce the kinetic frustration by accumulating phases that can effectively modify its hopping [26].

For $t' > 0$, it is not *a priori* obvious whether the FM state can survive in the ground state due to competing many-body effects. More formally, each matrix element satisfies $(\mathcal{H})_{ij} \geqslant 0$ under an appropriate gauge choice (see Sec. S1 of the Supplemental Material for details [36]). This violates Tasaki's criterion for NFM, which requires strictly nonpositive hopping matrix elements to ensure the fully spin-polarized ground state [35]. Instead, in this regime, the Perron-Frobenius theorem [37] guarantees a unique ferromagnetic state (apart from its trivial N-fold degeneracy) atop the many-body spectrum, but not necessarily as the ground state.

To analyze this, we investigate the instability of NFM against t' by introducing a single spin-flip into the fully polarized background. This simple ansatz provides a necessary condition for ferromagnetic instability, though it does not guarantee the true ground state—which we revisit later through full many-body DMRG calculations. The exact wavefunction of the single-hole Nagaoka state is represented by $|\psi\rangle_{1H} = \sum_j \alpha_j c_{j\uparrow} |\text{FM}\rangle$ (for some amplitude α_j) and that of the spin-flip (or one-hole-one-magnon, 1H1M) state by

$$|\psi\rangle_{1H1M} = \sum_{m\neq n} \alpha_{mn} c_{m\uparrow} S^-_n |\text{FM}\rangle\,, \quad (2)$$

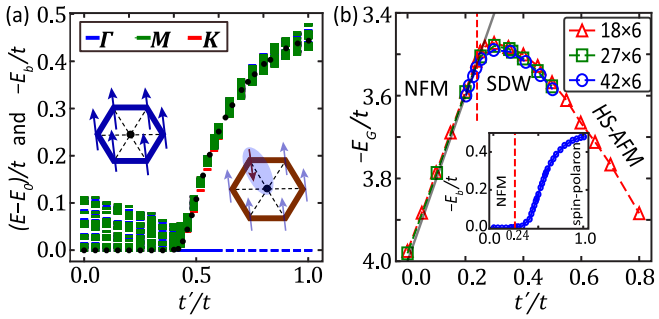

FIG. 2. (a) Exact low-lying energy spectra (dashed lines) of the hole-magnon system on 80×80 torus, shown relative to the ground-state energy E_0, as a function of t'/t for three center-of-mass momenta: $\mathbf{\Gamma} = (0, 0)$, $\mathbf{M} = (0, 2\pi/\sqrt{3})$, and $\mathbf{K} = (4\pi/3, 0)$. Black dots indicate the hole-magnon binding energy $(-E_b)$ on the same plot. Insets depict two competing regimes: A hole favoring Nagaoka FM (left), and a bound spin-polaron state emerging with increasing kinetic frustration (right). (b) Phase diagram and the ground-state energy of a hole vs t'/t for three different width-6 cylindrical clusters. The solid gray line shows the exact FM energy in the thermodynamic limit. Inset: hole-magnon binding energy on the same width-6 cylinders. Vertical red dashed lines mark the ground-state and spin-polaron transitions, both occurring near $t'/t \approx 0.24$.

for some scalar coefficients α_{mn}, where $S_n^- = c_{n\downarrow}^\dagger c_{n\uparrow}$ and $|\mathrm{FM}\rangle = \prod_{i=1}^N c_{i\uparrow}^\dagger |0\rangle$, with N being the number of sites. The condition $m \neq n$ ensures that a hole and a spin-flip do not occupy the same site. The instability is characterized by the hole-magnon binding energy, $E_b = E_{1\mathrm{H}1\mathrm{M}} - E_{1\mathrm{H}}$, where $E_{1\mathrm{H}}$ and $E_{1\mathrm{H}1\mathrm{M}}$ are the lowest energies of the 1H and 1H1M states, respectively. When $E_b < 0$, the FM state becomes unstable, and the spin-flip state emerges as an energetically favorable metastable configuration; otherwise, NFM remains stable and the binding energy must vanish, i.e., $E_b = 0$.

The 1H1M problem reduces to an effective tight-binding Hamiltonian in the relative coordinate (see Supplemental Material [36]). Building on the self-consistent method developed for the triangular lattice in Ref. [28], we extend it to the t-t' model and identify a hole-magnon bound state (spin polaron) that emerges above a dimension-dependent critical value t_c'. In 2D, the bound state at center-of-mass (COM) momentum $\mathbf{P} = \mathbf{0}$ follows from the inversion-odd representation and is given by (see derivations in Sec. S2 of the Supplemental Material [36])

$$[1 + t' f_{33}][1 + t(f_{11} + f_{12})] = 2tt' f_{13}^2, \tag{3}$$

where $f_{ij} = \frac{2}{N} \sum_{\boldsymbol{k} \in 1BZ} \frac{\sin(\boldsymbol{k}\cdot\boldsymbol{\delta}_i)\sin(\boldsymbol{k}\cdot\boldsymbol{\delta}_j)}{E - \epsilon_{\boldsymbol{k}}}$ is related to Fourier transform of coefficients α_{mn} and $\epsilon_{\mathbf{k}} = \sum_{\boldsymbol{\delta}} t_{\boldsymbol{\delta}} \cos(\mathbf{k} \cdot \boldsymbol{\delta})$ is the dispersion of bare hole (i.e., 1H) state, with $\boldsymbol{\delta}$ representing three neighboring vectors in triangular lattice [see Fig. 1(c)]. In the thermodynamic limit $N \to \infty$, Eq. (3) contains bound state solutions with energy E below the bare hole minima $(\epsilon_{\mathbf{k}}^{\min})$ for $t' > t_c' \approx 0.42t$. To visualize this, we calculate the many-body eigenenergy spectra and hole-magnon binding energy E_b via exact diagonalization on an 80×80 torus. For $t' < t_c'$, $E_b = 0$, indicating no bound state, while for $t' > t_c'$, negative E_b signals the spin-polaron formation [see Fig. 2(a) (black dots)], validating our analytic solution. This suggests that despite PHS and Tasaki's condition being broken, NFM remains stable up to a surprisingly large kinetic frustration. Above this critical value, the previously unbound hole-magnon pair localizes, with the bound spatial extent shrinking gradually as t' increases toward the triangular limit (see details in Sec. S3 of the Supplemental Material [36]). The bound state is strongest at $t' = 1$, with $E_b \approx 0.42t$, consistent with Ref. [28].

The 1H1M low-lying eigen spectra [dashed lines in Fig. 2(a)] further illustrate how kinetic frustration destabilizes NFM, forming a spin-polaron state. In the FM regime, $t' < t_c' \approx 0.42t$, magnon spectra appear as a continuum due to excitation gap scaling as $1/N$. However, above the critical t_c', the lowest-energy excitation is no longer a gapless magnon, but a composite spin polaron, which introduces a finite gap. The lowest-energy state shifts from COM $\mathbf{M}$ at small t' to $\mathbf{\Gamma}$ in the spin-polaron regime (also see Fig. S3 of the Supplemental Material [36]).

III. FRUSTRATION-INDUCED GROUND-STATE PHASE TRANSITION

To identify the true ground state at $U = \infty$, we now focus on the lowest $|S_z|$ sector. Using DMRG, we simulate width-6 cylinders with length along open boundary up to $L_x = 42$, allowing us to access longer-range correlations and reduce finite-size effects. The simulations are performed using the ITensor open-source library [38]. In Fig. 2(b), we show ground-state energies for three different cylinder lengths. It reveals a clear transition in the energy trend from linear to quadratic at $t' \approx 0.24t$, indicating a phase transition. The energy of the fully polarized state in the thermodynamic limit follows $E_G = 2t' - 4t$, which our data closely track for all clusters for $t' < 0.24t$, with only minor finite-size effects. We independently verify this phase boundary by examining the spin-polaron transition within the 1H1M sector on the same width-6 cylinders. As shown in the inset of Fig. 2(b), the results are in excellent agreement with the determined ground-state transition point. Although this transition point, $t' = 0.24t$, is close to the extrapolated thermodynamic limit found in a previous study [34], it is significantly smaller than our estimated 2D limit ($\sim 0.42t$) from the single spin-flip picture. We notice that for any finite-width cylinders, t_c' of the single hole-magnon system decreases as the cylinder width narrows and vanishes in the zigzag ladder limit (i.e., width-2 cylinder), which reflects a dimensional dependence of the Nagaoka state (see details in the Supplemental Material [36]). This situation is similar to the transition between stable and metastable Nagaoka FM with a change in the topology from 2D to one dimensional (1D), observed in quantum dot array [39], with a notable difference that the ground state in the zigzag ladder is a spin singlet ($S_{tot} = 0$), whereas in the 1D chain it is degenerate with the FM state.

To pin down the ground-state phase at various t', we calculate the spin correlation $C_{ij}^{\mathrm{ss}} = \langle \mathbf{S}_i \cdot \mathbf{S}_j \rangle$ and the static spin structure factor: $S(\mathbf{q}) = \frac{1}{N} \sum_{i,j} e^{i\mathbf{q}\cdot(\mathbf{r}_i - \mathbf{r}_j)} \langle \mathbf{S}_i \cdot \mathbf{S}_j \rangle$. In Figs. 3(a)–3(d), we show the real-space profile of C_{ij}^{ss}, represented by up and down arrows, with the reference site fixed at the center of the cluster (black dot). The color (and up/down orientation) of each arrow indicates the sign (blue

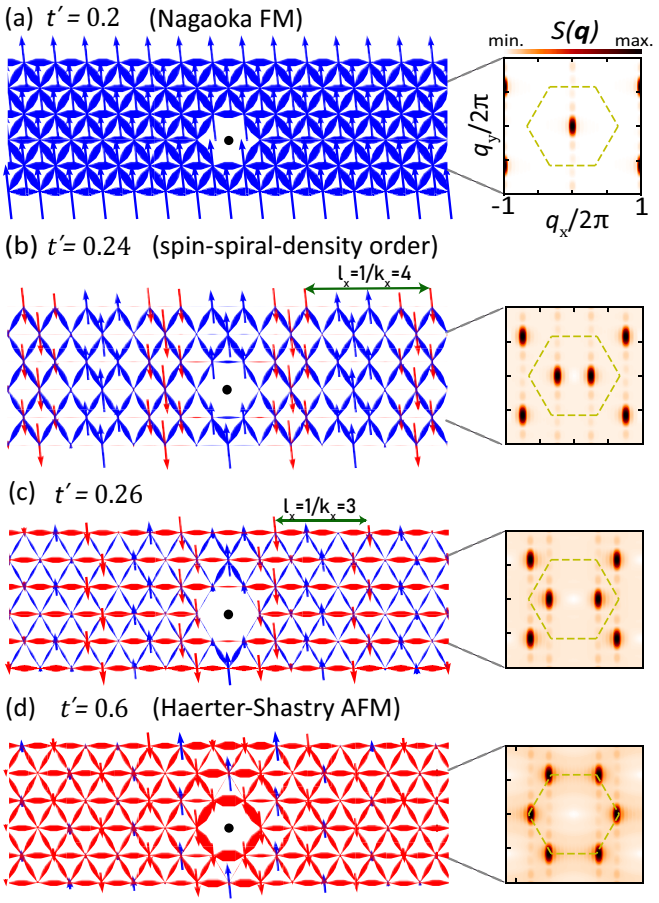

FIG. 3. Spin correlations profile and structure factor $S(\mathbf{q})$ for (a) Nagaoka FM at $t' = 0.2t$, (b) spiral spin wave at the transition point $t' = 0.24t$, (c) spiral order at $t' = 0.26t$, and (d) Haerter-Shastry AFM at $t' = 0.6t$. Up/down arrows indicate spin correlation $\langle \mathbf{S}_i \cdot \mathbf{S}_o \rangle$ relative to a fixed reference site (black dot); arrow length indicates magnitude and color indicates sign (blue: positive; red: negative). Bond thickness shows quantum snapshots of spin correlations between neighboring sites obtained by freezing the hole at the center (black dot). Bond colors follow the same sign convention. The dashed hexagon in $S(\mathbf{q})$ represents the Brillouin zone of the triangular lattice. All results are for one hole in $S_z = 1/2$ sector, computed via DMRG on an 18×6 cylinder with bond dimension up to $D = 14\,000$ and truncation error below 2×10^{-6}.

for positive, red for negative), while the arrow length reflects the magnitude of $C^{\rm ss}_{ij}$. The corresponding $S(\mathbf{q})$ is shown in the rightmost panel of each figure. At $t'/t = 0.2$ [Fig. 3(a)], below the transition point, spin correlations are saturated to their maximum value $\sim\frac{N-1}{4N}$ (each arrow length is $\sim$0.247) and the Bragg peak appears at the center of the Brillouin zone (BZ) $\mathbf{\Gamma}$, with the peak amplitude close to the expected value $S(\mathbf{\Gamma}) \approx 26.99$, corresponding to a saturated FM on the 18×6 cluster. This NFM survives until the transition point, as evident from the linear energy fit in Fig. 2(b). At the transition point, $t'/t = 0.24$, the competing FM and AFM correlations lead to an alternating-sign pattern in the spin correlation $C^{\rm ss}_{ij}$, forming multiple ferromagnetic domains [Fig. 3(b)]. This critical state is a spiral spin wave order with a wavelength of $l_x \approx 4$ lattice constants in our finite-width geometry. The associated Bragg peak splits to the ordering vectors $\boldsymbol{q} \approx (\pm\pi/2, 0)$, perfectly consistent with the spiral pitch with wavelength being $l_x \approx 4$. As t' is increased above t'_c [Fig. 3(c)], the spiral spin wavelength reduces and associated Bragg peaks gradually evolves toward the BZ corners, approaching $\sqrt{3} \times \sqrt{3}$ chiral spin order in the Haerter-Shastry AFM regime at $t' = 0.6t$ and above [Fig. 3(d)].

Local magnetic bond correlations around a dopant are often useful in cold-atom experiments at finite, but large, U in understanding competing magnetic orders [15,16]. In the large-U limit, the superexchange mechanism is suppressed near the dopant, and kinetic effects in the vicinity of the hole become locally accessible. To probe this local competition between FM and AFM correlations, we also show the normalized hole-spin-spin correlation $C^{\rm hss}_{ij} = \langle h_0^\dagger \boldsymbol{S}_i \cdot \boldsymbol{S}_j h_0 \rangle / \langle h_0^\dagger h_0 \rangle$ in the ground state, where $h_0 = c_{0\downarrow} c^\dagger_{0\downarrow} c_{0\uparrow} c^\dagger_{0\uparrow}$ pins a hole at the central site "0". Figures 3(a)–3(d) show the nearest-neighbor $C^{\rm hss}_{ij}$, visualized using bond thickness to indicate magnitude and color (blue for FM, red for AFM) to indicate sign, with the hole frozen at the center of the cluster (black dot). At $t'/t = 0.2$, all bond correlations are positive, as expected for NFM. However, at the transition point $t'/t = 0.24$, spin correlations are FM along each square plaquette, while correlations along horizontal bonds vanish. This critical behavior indicates the onset of the kinetic frustration effect as increasing t' introduces competing hole paths that frustrate the FM alignment and prevent all bonds from being simultaneously satisfied. As t' is increased further, these horizontal bonds reverse sign and become antiferromagnetic [Fig. 3(c)]. Enhanced AFM bonds around the dopant in Fig. 3(d) reflect the hole's growing tendency to favor local AFM alignments under stronger kinetic frustration.

IV. FINITE-HOLE DOPING EFFECTS

After gaining insights from a single-hole dopant, we now investigate finite-hole doping as it is more relevant to experiments. While the NFM state on a square lattice is often debated as a singular-hole artifact, recent analytical and numerical evidence suggests it can persist as a robust thermodynamic phase at finite doping. Rigorous results for the two-hole sector [40] establish a mathematical foundation for finite-hole NFM in the thermodynamic limit, while state-of-the-art many-body simulations—including unbiased DMRG and fermionic quantum Monte Carlo—consistently predict a persistent ferromagnetic ground state up to a critical doping of $\delta \approx 0.2$ [41–43]. The potential for such states to manifest in quantum dots and cold-atom systems gives these findings significant experimental weight, regardless of whether the effects are truly thermodynamic or limited to large, finite-sized clusters. Despite these advances, the resilience of NFM against the competing effects of kinetic frustration remains largely unexplored.

We use DMRG simulation to characterize the ground state and its evolution under t' hopping at hole densities $\delta \approx 0.06$ (6 holes) and $\delta \approx 0.11$ (12 holes) on 18×6 cylinders. Finite doping poses significant convergence challenges, requiring bond dimensions up to $D = 25\,000$, with $U(1)$ symmetry to control truncation errors below 1×10^{-5}. In Fig. 4(a), we show the $S(\mathbf{q})$ with cut along $q_y = 0$ for $\delta \approx 0.11$ at

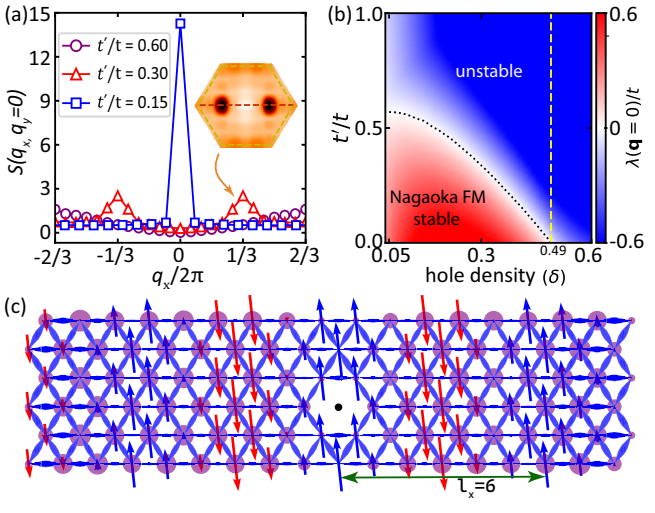

FIG. 4. (a) Ground state $S(\mathbf{q})$ along $\mathbf{q}_y = 0$ (marked by the horizontal red dashed line in the inset), obtained by considering bulk 72 sites, for 12 holes on 18×6 cylinders. Inset: full $S(\mathbf{q})$ within the first BZ. (b) Excitation energy at band bottom $\mathbf{q} = (0, 0)$ as a function of hole density and anisotropy t'/t, obtained from the SKA variational solution. The dotted black line represents the boundary below which the Nagaoka phase is stable. The yellow dashed line at $\delta = 0.49$ indicates the critical density above which NFM is unstable. (c) The real space spin and bond correlation profile for six holes on 18×6 cluster near transition at $t' = 0.25t$. Plotting conventions follow Fig. 3. The size of the purple dots indicates the strength of hole-hole correlations relative to the central site (black dot).

representative values of t'. At $t' = 0.15t$, the Bragg peak at $\mathbf{\Gamma}$ (i.e., $q_x = 0$) reaches a saturation value $S(\mathbf{\Gamma}) \approx 14.66$ for the bulk 72 sites of the cluster, confirming NFM. At $t' = 0.3t$, the Bragg peak splits, similar to the single-dopant case, forming spiral spin density order with ordering vector $q_x = \pm 2\pi/3$. This corresponds to the real-space periodicity $l_x = 3$. However, this wavelength is longer compared to the single-hole dopant case, indicating a modified magnetic response at finite doping. A similar effect appears at low doping $\delta \approx 0.06$ [Fig. 4(c)], where the periodicity extends to $l_x = 6$ near the transition. This longer periodicity arises from the effective repulsion between holes, as seen in the hole-hole correlation (purple dots), where each hole prefers its own FM background, avoiding overlap with others. This is evident from the vanishing hole correlation along the central stripe (blue arrows) where a reference hole is fixed at the center (black dot). At both doping δ, we find 120° AFM states with peaks at $q_x = \pm 4\pi/3$ at larger t' values, akin to the single-hole dopant case.

Due to the lack of an exact solution for finite hole density, even in the simplest scenario of a single spin-flip, we adopt the variational wavefunction approach introduced by Shastry, Krishnamurthy, and Anderson (SKA) [44] to elucidate further the physical origin of instability NFM due to kinetic frustration. Originally, the SKA method was developed to analyze the "k_F instability" of NFM under finite doping. While the SKA approach is known to overestimate Nagaoka stability, it effectively captures the key instability mechanism, offering valuable insights where direct numerical simulations are computationally demanding across multiple δ and t'. The SKA wavefunction describes the leading instability as an overturned (spin-flip) electron from the Fermi surface of the fully polarized state and creating a down-spin electron at the band bottom:

$$|\psi_v(\mathbf{q})\rangle = \frac{1}{\sqrt{N}} \sum_j e^{i\mathbf{q}\cdot\mathbf{r}_j} c^\dagger_{j\downarrow} (1 - n_{j\uparrow}) c_{\mathbf{k}_F\uparrow} |F\rangle , \qquad (4)$$

where $|F\rangle = \prod_{0 \leqslant |\mathbf{k}| \leqslant \mathbf{k}_F} c^\dagger_{\mathbf{k}\uparrow} |\text{vac}\rangle$ is the FM state at finite hole density and $\mathbf{k}_F$ is one of the Fermi surface vectors. The projector $1 - n_{j\uparrow}$ in Eq. (4) enforces the $U = \infty$ constraint in real space. This allows us to switch off U and leverage the Hamiltonian to noninteracting model, $H = -\sum_{\langle i,j\rangle} t_{ij} c^\dagger_{i\sigma} c_{j\sigma}$. The excitation energy is then given by

$$\lambda(\mathbf{q}) = \frac{\langle\psi_v| (H - E_o) |\psi_v\rangle}{\langle\psi_v|\psi_v\rangle}, \qquad (5)$$

where E_o is the energy of the polarized state. A straightforward but lengthy calculation gives

$$\lambda(\mathbf{q}) = \mu - \epsilon_{\mathbf{k}_F} + \epsilon_{\mathbf{q}}\delta + \frac{1}{\delta N^2} \sum_{i,j} t_{ij} e^{i\mathbf{q}\cdot\mathbf{r}_{ij}} \left| \sum_{\mathbf{k}} e^{i\mathbf{k}\cdot\mathbf{r}_{ij}} \langle n_{\mathbf{k}\uparrow}\rangle \right|^2 , \qquad (6)$$

where $\mu = -\frac{E_o}{N\delta}$ and $\epsilon_{\mathbf{q}} = -\frac{1}{N}\sum_{i,j} t_{ij} e^{i\mathbf{q}\cdot\mathbf{r}_{ij}}$, with $\mathbf{r}_{ij} = \mathbf{r}_i - \mathbf{r}_j$. For isotropic case, $t_{ij} = t$, the last integral term simplifies to $-\epsilon_{\mathbf{q}}\delta(\frac{\mu}{zt})^2$, where z is the coordination number. Since the sixfold rotational symmetry is broken in our anisotropic case, we solve Eq. (6) numerically. The first two terms, $\mu - \epsilon_{\mathbf{k}_F} \geqslant 0$, capture the net energy cost for up electrons needed to avoid the inserted down electron. The remaining last two terms, proportional to $\epsilon_{\mathbf{q}}$, account for the energy gain from the delocalized down electron.

To find the minimum excitation energy, we replace $\epsilon_{\mathbf{q}}$ by the band bottom energy $\epsilon_{\mathbf{q}=\mathbf{0}}$, as band minima occur at $\mathbf{q} = \mathbf{0}$ for all $t' > 0$. The interplay between hole density δ and t' modifies the magnon's effective band curvature. When either parameter increases, the band steepens, eventually leading to the "k_F instability" of NFM, as illustrated in Fig. 4(b). At $\delta = 0.05$, the instability occurs around $t' \approx 0.57t$, which is higher than our estimated critical value $t'_c \approx 0.42t$ for a single hole in the thermodynamic limit. This discrepancy represents the inadequacy of the mean-field SKA ansatz in incorporating the exact correlation effects among constituents. Further increasing δ enhances the curvature, shifting the instability to lower t', and NFM ultimately vanishes below $\delta \approx 0.49$.

V. CONCLUSIONS

We have explored the instability of Nagaoka ferromagnet and the resulting quantum phase transition by controlling dopants' kinetic frustration via tuning the lattice geometry between square and triangular limits. Combining analytical insights with large-scale numerical simulations, we have identified the microscopic origin of this instability both in the single-hole limit and at finite hole density. Since Nagaoka ferromagnetism at finite doping is stabilized by a macroscopic kinetic energy gain [45], it remains robust against moderate perturbations such as kinetic frustration (t'/t) and strong on-site repulsion (U), establishing it as a realistic many-body

phenomenon rather than just a pathological feature of the single-hole limit. Beyond the Nagaoka regime, signatures of ground-state quantum phase transitions—identified through local magnetic correlations—indicate that competing magnetic tendencies yield critical behavior with a spiral spin density phase that connects the Nagaoka and Haerter-Shastry limits. These local magnetic correlations and the critical role of kinetic frustration could be directly probed in future cold-atom experiments and moiré Hubbard platforms. In such settings, our analysis can be extended to a finite but large-U regime on tunable square-triangular lattices, where itinerant holes locally suppress the superexchange mechanism.

ACKNOWLEDGMENTS

We thank S. Sherif for discussions on related work. This work was primarily supported by the U.S. Department of Energy (DOE), Office of Science, Basic Energy Sciences, under Early Career Award No. DE-SC0024524. H.J.C. acknowledges funding from the National Science Foundation (NSF) Grant No. DMR 2046570 under the CAREER program, and the National High Magnetic Field Laboratory (NHMFL). The NHMFL is supported by NSF/DMR-2128556 and the state of Florida. Y.P. was supported by NSF Grants No. PHY-2216774 and No. DMR-2406524. D.N.S. was supported by the U.S. DOE, Office of Basic Energy Sciences under Grant No. DE-FG02-06ER46305. The simulation used resources of the National Energy Research Scientific Computing Center, a U.S. Department of Energy Office of Science User Facility located at Lawrence Berkeley National Laboratory, operated under Contract No. DE-AC02-05CH11231, and local computing resources yquantum at CSUN, and Planck at FSU.

DATA AVAILABILITY

The data that support the findings of this article are openly available [46].

[1] Y. Nagaoka, Ferromagnetism in a narrow, almost half-filled *s* band, Phys. Rev. **147**, 392 (1966).
[2] D. Thouless, Exchange in solid ^{3}He and the Heisenberg Hamiltonian, Proc. Phys. Soc. **86**, 893 (1965).
[3] E. C. Stoner, Collective electron ferromagnetism, Proc. R. Soc. London A **165**, 372 (1938).
[4] A. L. Sharpe, E. J. Fox, A. W. Barnard, J. Finney, K. Watanabe, T. Taniguchi, M. Kastner, and D. Goldhaber-Gordon, Emergent ferromagnetism near three-quarters filling in twisted bilayer graphene, Science **365**, 605 (2019).
[5] K. R. Kittilstved, D. A. Schwartz, A. C. Tuan, S. M. Heald, S. A. Chambers, and D. R. Gamelin, Direct kinetic correlation of carriers and ferromagnetism in Co^{2+}:ZnO, Phys. Rev. Lett. **97**, 037203 (2006).
[6] K. F. Mak and J. Shan, Semiconductor moiré materials, Nat. Nanotechnol. **17**, 686 (2022).
[7] F. Wu, T. Lovorn, E. Tutuc, and A. H. MacDonald, Hubbard model physics in transition metal dichalcogenide moiré bands, Phys. Rev. Lett. **121**, 026402 (2018).
[8] K. P. Nuckolls and A. Yazdani, A microscopic perspective on moiré materials, Nat. Rev. Mater. **9**, 460 (2024).
[9] S. Xie *et al.*, Strong interlayer interactions in bilayer and trilayer moiré superlattices, Sci. Adv. **8**, eabk1911 (2022).
[10] C. Zener, Interaction between the *d*-shells in the transition metals. II. Ferromagnetic compounds of manganese with perovskite structure, Phys. Rev. **82**, 403 (1951).
[11] Y. Tokura and N. Nagaosa, Orbital physics in transition-metal oxides, Science **288**, 462 (2000).
[12] E. Dagotto, T. Hotta, and A. Moreo, Colossal magnetoresistant materials: The key role of phase separation, Phys. Rep. **344**, 1 (2001).
[13] Y. Tang *et al.*, Simulation of Hubbard model physics in WSe_2/WS_2 moiré superlattices, Nature (London) **579**, 353 (2020).
[14] L. Ciorciaro *et al.*, Kinetic magnetism in triangular moiré materials, Nature (London) **623**, 509 (2023).
[15] M. L. Prichard, B. M. Spar, I. Morera, E. Demler, Z. Z. Yan, and W. S. Bakr, Directly imaging spin polarons in a kinetically frustrated Hubbard system, Nature (London) **629**, 323 (2024).
[16] M. Lebrat, M. Xu, L. H. Kendrick, A. Kale, Y. Gang, P. Seetharaman, I. Morera, E. Khatami, E. Demler, and M. Greiner, Observation of Nagaoka polarons in a Fermi–Hubbard quantum simulator, Nature (London) **629**, 317 (2024).
[17] J. Koepsell, J. Vijayan, P. Sompet, F. Grusdt, T. A. Hilker, E. Demler, G. Salomon, I. Bloch, and C. Gross, Imaging magnetic polarons in the doped Fermi–Hubbard model, Nature (London) **572**, 358 (2019).
[18] K. Lee, P. Sharma, O. Vafek, and H. J. Changlani, Triangular lattice Hubbard model physics at intermediate temperatures, Phys. Rev. B **107**, 235105 (2023).
[19] I. Morera, M. Kanász-Nagy, T. Smolenski, L. Ciorciaro, A. Imamoğlu, and E. Demler, High-temperature kinetic magnetism in triangular lattices, Phys. Rev. Res. **5**, L022048 (2023).
[20] R. Samajdar and R. N. Bhatt, Nagaoka ferromagnetism in doped Hubbard models in optical lattices, Phys. Rev. A **110**, L021303 (2024).
[21] M. Xu, L. H. Kendrick, A. Kale, Y. Gang, G. Ji, R. T. Scalettar, M. Lebrat, and M. Greiner, Frustration- and doping-induced magnetism in a Fermi–Hubbard simulator, Nature (London) **620**, 971 (2023).
[22] G. Li, A. E. Antipov, A. N. Rubtsov, S. Kirchner, and W. Hanke, Competing phases of the Hubbard model on a triangular lattice: Insights from the entropy, Phys. Rev. B **89**, 161118(R) (2014).
[23] D. Pereira and E. J. Mueller, Kinetic magnetism in the crossover between the square and triangular lattice Fermi-Hubbard models, Phys. Rev. B **112**, 245120 (2025).
[24] Y. Zhang and L. Fu, Pseudogap metal and magnetization plateau from doping moiré Mott insulator, SciPost Phys. Core **6**, 038 (2023).
[25] J. O. Haerter and B. S. Shastry, Kinetic antiferromagnetism in the triangular lattice, Phys. Rev. Lett. **95**, 087202 (2005).

[26] C. N. Sposetti, B. Bravo, A. E. Trumper, C. J. Gazza, and L. O. Manuel, Classical antiferromagnetism in kinetically frustrated electronic models, Phys. Rev. Lett. **112**, 187204 (2014).

[27] G. Martinez and P. Horsch, Spin polarons in the *t*-*J* model, Phys. Rev. B **44**, 317 (1991).

[28] M. Davydova, Y. Zhang, and L. Fu, Itinerant spin polaron and metallic ferromagnetism in semiconductor moiré superlattices, Phys. Rev. B **107**, 224420 (2023).

[29] S.-S. Zhang, W. Zhu, and C. D. Batista, Pairing from strong repulsion in triangular lattice Hubbard model, Phys. Rev. B **97**, 140507(R) (2018).

[30] R. C. Newby and E. Khatami, Finite-temperature kinetic ferromagnetism in the square-lattice Hubbard model, Phys. Rev. B **111**, 245120 (2025).

[31] Z. Tao, W. Zhao, B. Shen, T. Li, P. Knüppel, K. Watanabe, T. Taniguchi, J. Shan, and K. F. Mak, Observation of spin polarons in a frustrated moiré Hubbard system, Nat. Phys. **20**, 783 (2024).

[32] W. Barford and J. H. Kim, Spinless fermions on frustrated lattices in a magnetic field, Phys. Rev. B **43**, 559 (1991).

[33] J. Merino, B. J. Powell, and R. H. McKenzie, Ferromagnetism, paramagnetism, and a Curie-Weiss metal in an electron-doped Hubbard model on a triangular lattice, Phys. Rev. B **73**, 235107 (2006).

[34] F. T. Lisandrini, B. Bravo, A. E. Trumper, L. O. Manuel, and C. J. Gazza, Evolution of Nagaoka phase with kinetic energy frustrating hopping, Phys. Rev. B **95**, 195103 (2017).

[35] H. Tasaki, Extension of Nagaoka's theorem on the large-U Hubbard model, Phys. Rev. B **40**, 9192 (1989).

[36] See Supplemental Material at https://link.aps.org/supplemental/10.1103/z4gs-c6h6 for detailed derivation of kinetic magnetism in triangular geometry, analytic solution for one-hole-one-magnon states in 1D and 2D limits, and the probability distribution of the one-hole-one-magnon states.

[37] S. U. Pillai, T. Suel, and S. Cha, The Perron-Frobenius theorem: Some of its applications, IEEE Signal Process. Mag. **22**, 62 (2005).

[38] M. Fishman, S. R. White, and E. M. Stoudenmire, The itensor software library for tensor network calculations, SciPost Phys. Codebases 4 (2022).

[39] I. Ivantsov, H. B. Xavier, A. Ferraz, and E. Kochetov, Stable and metastable kinetic ferromagnetism on a ring, Phys. Rev. B **101**, 195107 (2020).

[40] G.-S. Tian, The Nagaoka state in the one-hand Hubbard model with two and more holes, J. Phys. A: Math. Gen. **24**, 513 (1991).

[41] G. Carleo, S. Moroni, F. Becca, and S. Baroni, Itinerant ferromagnetic phase of the Hubbard model, Phys. Rev. B **83**, 060411(R) (2011).

[42] L. Liu, H. Yao, E. Berg, S. R. White, and S. A. Kivelson, Phases of the infinite U Hubbard model on square lattices, Phys. Rev. Lett. **108**, 126406 (2012).

[43] X. Y. Zhang, E. Abrahams, and G. Kotliar, Quantum Monte Carlo algorithm for constrained fermions: Application to the infinite-U Hubbard model, Phys. Rev. Lett. **66**, 1236 (1991).

[44] B. S. Shastry, H. R. Krishnamurthy, and P. W. Anderson, Instability of the Nagaoka ferromagnetic state of the $U = \infty$ Hubbard model, Phys. Rev. B **41**, 2375 (1990).

[45] F. Becca and S. Sorella, Nagaoka ferromagnetism in the two-dimensional infinite-U Hubbard model, Phys. Rev. Lett. **86**, 3396 (2001).

[46] P. Sharma, Y. Peng, D. Sheng, H. Changlani, and Y. Wang, Instability of nagaoka state and quantum phase transition via kinetic frustration control [Data set], Zenodo (2026), doi: 10.5281/zenodo.19297472.